International Journal of Nanoelectronics and Materials
Volume 14 (Special Issue) December 2021 [11-19]

UniMAP UNIVERSITI MALAYSIA PERLIS

Ohmic Contacts Optimisation for High-Power InGaAs/AlAs Double-Barrier Resonant Tunnelling Diodes Based on a Dual-Exposure E-Beam Lithography Approach

Davide Cimbri[1*], Nils Weimann[2], Qusay Raghib Ali Al-Taai[1], Afesomeh Ofiare[1], and Edward Wasige[1]

[1] High-Frequency Electronics group, division of Electronics and Nanoscale Engineering, James Watt School of Engineering, University of Glasgow, G12 8LT, Glasgow, United Kingdom.
[2] Components for High Frequency Electronics (BHE), department of Electrical Engineering and Information Technology, University of Duisburg-Essen, 47057, Duisburg, Germany.

ABSTRACT

In this paper, we report on a simple test structure which can be used to accurately extract the specific contact resistivity ρ_c associated with metal-n++ InGaAs-based low-resistance Ohmic contacts through the transfer length method (TLM). The structure was designed to avoid common measurement artifacts that typically affect standard layouts. Moreover, microfabrication was optimised to achieve an accurate short minimum gap spacing of 1 μm through a dual-exposure step based on e-beam lithography, which is required for a reliable ρ_c estimation. Ohmic contacts based on a Ti/Pd/Au metal stack were fabricated and characterised using the proposed structure, resulting in an extracted $\rho_c \simeq 1.37\times10^{-7}\ \Omega\ cm^2 = 13.7\ \Omega\ \mu m^2$. This work will assist in increasing the quality of Ohmic contacts in high-power InGaAs/AlAs double-barrier resonant tunnelling diodes (RTDs), and so help to overcome one of the bottlenecks to the output power capability of RTD-based oscillators at terahertz frequencies.

Keywords: Specific contact resistivity, transfer length method, e-beam lithography, Ohmic contact, resonant tunnelling diode, terahertz oscillator.

1. INTRODUCTION

Resonant tunnelling diodes (RTDs) [1] are sparking great interest as a potential technology for next-generation ultra-high-speed sources [2] and detectors [3] which will work in the terahertz (THz) frequency band (0.1-10 THz) [4]. Among the several issues that still prevent RTD-based emitters to be employed in practical application scenarios [5], the parasitic resistance R_c associated with Ohmic contacts is one of the main factors which limit the RF power capability of the RTD device at high-frequency [6]. In particular, the specific contact resistivity ρ_c imposes an upper boundary to the diode cut-off frequency, limiting the maximum oscillation frequency at which the RTD device can provide RF gain [7], and limits the maximum output power that the diode is able to deliver to a load at a specific operation frequency [8]. For high-power indium gallium arsenide/aluminium arsenide (InGaAs/AlAs) double-barrier RTDs aimed at oscillator design in the low-THz range (~ 100-300 GHz) [9], this is currently mainly caused by the unoptimised metal-to-semiconductor junction fabrication process, which still keeps ρ_c far from physical limiting values [10] [11], resulting in poor Ohmic contacts. However, Ohmic contact optimization requires an accurate and reliable approach to experimentally extract ρ_c, which hasn't yet been developed in this context.
In this paper, we propose a simple test structure that can be employed to accurately estimate ρ_c associated with metal-*n*++ InGaAs-based low-resistance Ohmic contacts by means of the transfer length method (TLM) [12]. The structure was carefully designed to avoid common measurement

*davide.cimbri@glasgow.ac.uk

artifacts [13] that typically affect standard layouts. Moreover, microfabrication was optimised to achieve an accurate short minimum gap spacing of 1 μm by means of a dual-exposure step based on electron-beam (e-beam) lithography (EBL), which is required for a reliable ρ_c estimation. Ohmic contacts based on a titanium/palladium/gold (Ti/Pd/Au) metal stack were fabricated and characterised using the developed structure, resulting in an extracted $\rho_c \simeq 1.37\times10^{-7}$ Ω cm^2 = 13.7 Ω μm^2). Details about this work are described in the following sections.

2. DESIGN OF THE TLM STRUCTURE

The proposed TLM structure is shown in Figure 1, featuring gap spacing ranging from 6 μm down to 1 μm for accurate ρ_c extraction. A simple linear geometry was adopted to simplify the design process. In this regard, circular geometries [14] are widely used since they only require one lithographic step and do not suffer from in-plane current crowding effects [15]. However, state-of-the-art TLM structures used to estimate ρ_c associated with InGaAs-based Ohmics employ linear designs optimised for four-point probe sensing [16]. Indeed, fringing currents can be easily eliminated via structure insulation through wet etching on top of a semi-insulating (SI) substrate by means of accurate mask alignment, avoiding more complex design strategies [17]. Separate probe landing areas were designed and positioned far from the gaps [18] to avoid measurement artifacts arising in standard square-based structures due to variations in manual probes positioning, which are well-known to give random measurement fluctuations, and unrepeatable and unreliable ρ_c extraction [13]. At the same time, metal interconnections were designed to reduce the associated parasitic resistance by employing a large patch width of 80 μm.
EBL was chosen to pattern the structure due to the unreliability of optical-lithography in the case of the 1 μm wide gap opening, which gives low reproducibility and needs careful scanning electron microscope (SEM) analysis after lift-off for each structure and at each fabrication run to remove any possible source of unwanted systematic error. Due to reflection phenomena occurring in proximity to the gaps during e-beam exposure, the resist profile typically takes a positive symmetric curved shape at both edges after development, resulting in a smaller equivalent gap width and, for short ones, complete gap closure after lift-off. Although this can be easily sorted by reducing the exposure dose, it results in the patterned regions to be left underexposed. To solve this issue, a dual-exposure process using two different doses was proposed. A first high-dose layer associated with the correct dose for reliable gaps shaping and opening was designed to cover the entire TLM structure, while a second low-dose one was superimposed to the first, to compensate for underexposure, by keeping a distance of 6 μm from the gaps. Moreover, the mesa was shaped for fringing currents suppression by surrounding the whole structure with a tolerance of + 0.5 μm, which is the resolution of the employed photo-resist.

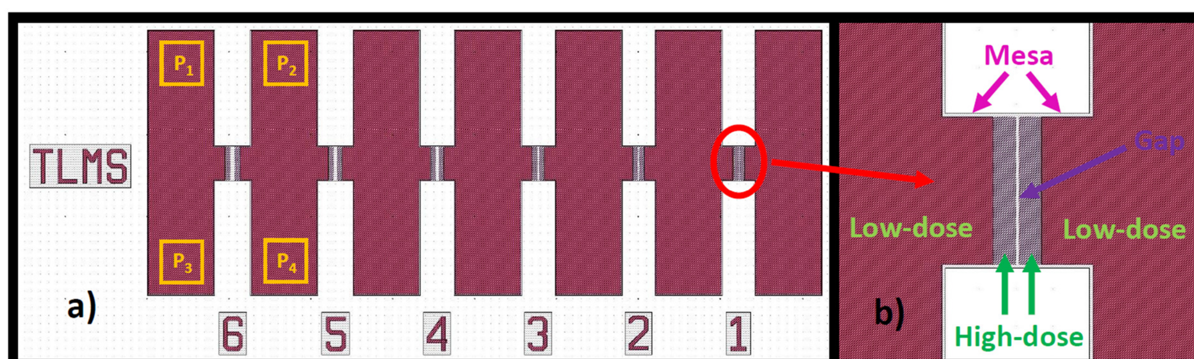

Figure 1. Design of the TLM structure, featuring gap spacing ranging from 6 μm to 1 μm. In **a)**, the layout of the structure, showing probes landing areas. In **b)**, a zoom in over the 1 μm wide gap area, outlining high/low-dose regions and mesa.

3. FABRICATION OF THE TLM STRUCTURE

The fabrication process comprised of one e-beam and one optical-lithographic step, for a total of eight steps. A schematic of the fabrication process is depicted in Figure 2 and explained in the following:

i) *Sample*: the ~ 1.2×1.2 cm^2 large sample consisted of a ~ 930 nm thick $In_{0.53}Ga_{0.47}As$/AlAs double-barrier heterostructure lattice matched with indium phosphide, featuring a 40 nm thick heavily silicon (Si)-doped n++ $In_{0.53}Ga_{0.47}As$ cap layer with donor concentration N_D ~ 3×10^{19} cm^{-3}, which was epitaxially grown on top of a 650 μm thick SI InP substrate by IQE.

1) *E-beam resist spin coating and exposure*: a dual positive e-beam resist (PMMA-based) thin layer was spun onto the sample surface and patterned through EBL by means of a dual-exposure process. The high and low doses were set to 490 and 310, respectively. A total of one hundred and twelve structures were patterned.

2) *E-beam resist development and surface de-oxidation*: the resist was developed and the InGaAs surface de-oxidised prior to metal deposition. In particular, in this work, the sample was exposed to ozone (O_3) under UV light for 4 min and 30 s and then treated using a hydrochloric acid-based dilute solution (HCl:H_2O=1:3) for 5 min. Figure 3 a) and b) show photomicrographs of a test structure after development. As it is possible to see, the backbone of the structure was correctly exposed and developed. Moreover, all the gaps, including the 1 μm wide, were correctly processed, revealing a straight profile.

3) *Metal deposition*: metal was deposited through electron-beam physical vapour deposition (EBPVD). In particular, Ti/Pd/Au=20/30/150 nm were evaporated in this work. The time occurring between sample de-oxidation and chamber pumping was ~ 50 s.

4) *Lift-off*: metal dual lift-off was carried out. Figure 4 a) and b) show photomicrographs of a test structure after lift-off. As it is possible to notice, the metal was successfully patterned, and the gaps opened. To double-check it, a SEM analysis was performed on different structures, randomly selected across the sample, to obtain statistical significance. The analysis focused on the 1 μm wide gap (being the critical one) by measuring the gap width at different lateral positions. For instance, Figure 4 c) and d) report SEM images of the 1 μm wide gap belonging to one of the analysed structures. The investigation confirmed the correct opening of the gaps, with a tolerance of ≃ ± 50-60 nm between the different structures, which allows for a reliable ρ_c extraction.
Metal corrugation was observed at the gaps edges perpendicularly with the sample surface, as reported in Figure 4 d). This is explained by the presence of deposited metal on top of the resist later sidewalls caused by the isotropic nature of evaporation, resulting in metal flakes left along the surface edges in close proximity to the gaps. Despite that, this does not affect the reliability of the extraction process, since the actual gap width is measured at the InGaAs surface, where SEM imaging confirmed the gap edges to be smooth.

5) *Photo-resist spin coating and exposure*: a positive photo-resist (S1800-based) thin layer was spun and patterned through optical-lithography.

6) *Photo-resist development and sample ashing*: the photo-resist was developed and the sample ashed at 80 W for 2 min.

7) *Wet etching*: the mesa was defined and the structures electrically insulated from the surrounding by means of chemical wet etching (H_3PO_4:H_2O_2:H_2O=1:1:38) with rate of ~ 100 nm/min up to the SI InP substrate, for a total dip time of 10 min.

8) *Photo-resist stripping*: the resist was stripped, finalising the fabrication process.

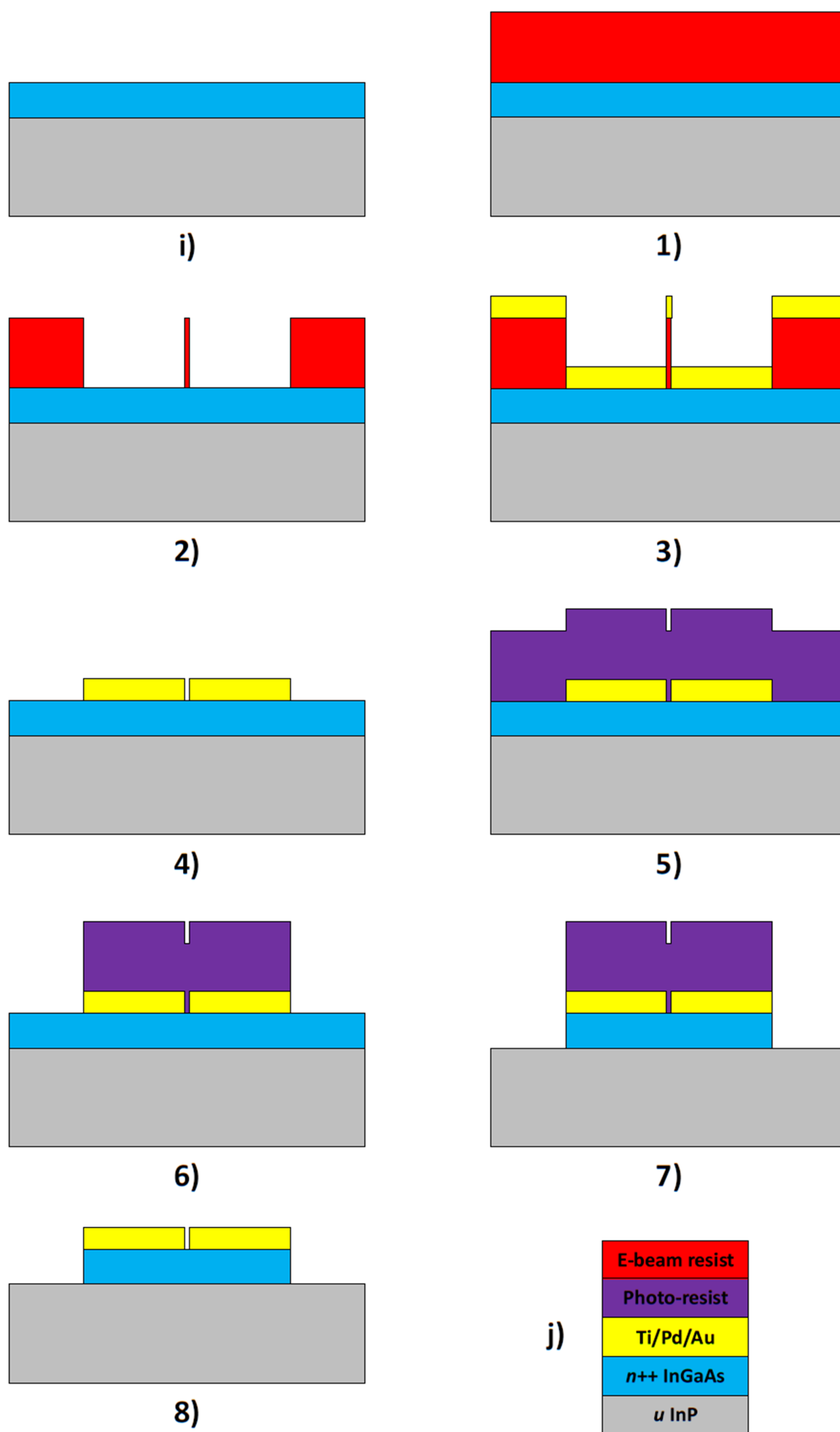

Figure 2. Schematic of the TLM structure fabrication process: **i)** *sample*, **1)** *e-beam resist spin coating and exposure*, **2)** *e-beam resist development and surface de-oxidation*, **3)** *metal deposition*, **4)** *lift-off*, **5)** *photo-resist spin coating and exposure*, **6)** *photo-resist development and sample ashing*, **7)** *wet etching*, **8)** *photo-resist stripping*, **j)** *legend*.

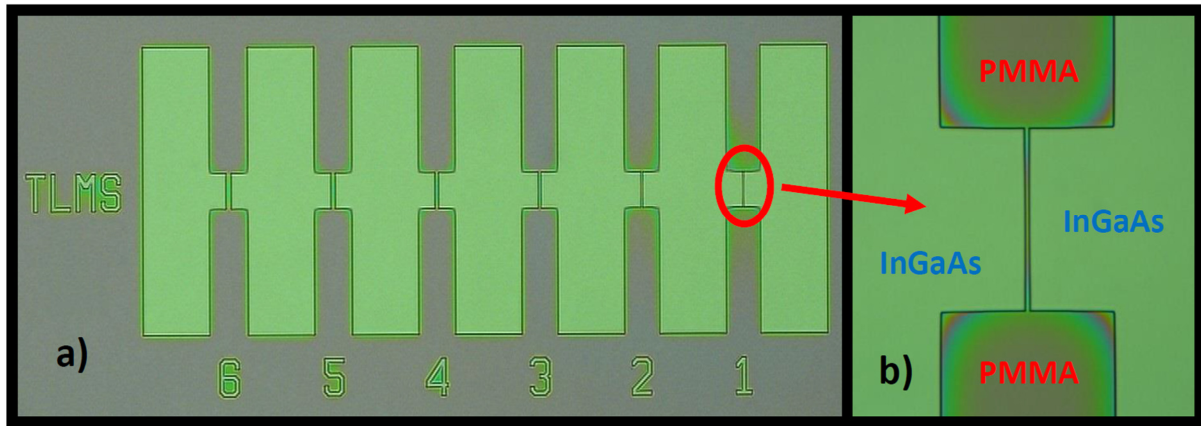

Figure 3. Photomicrographs of a TLM structure after e-beam resist development. In **a)**, the whole structure. In **b)**, a zoom in over the 1 μm wide gap area.

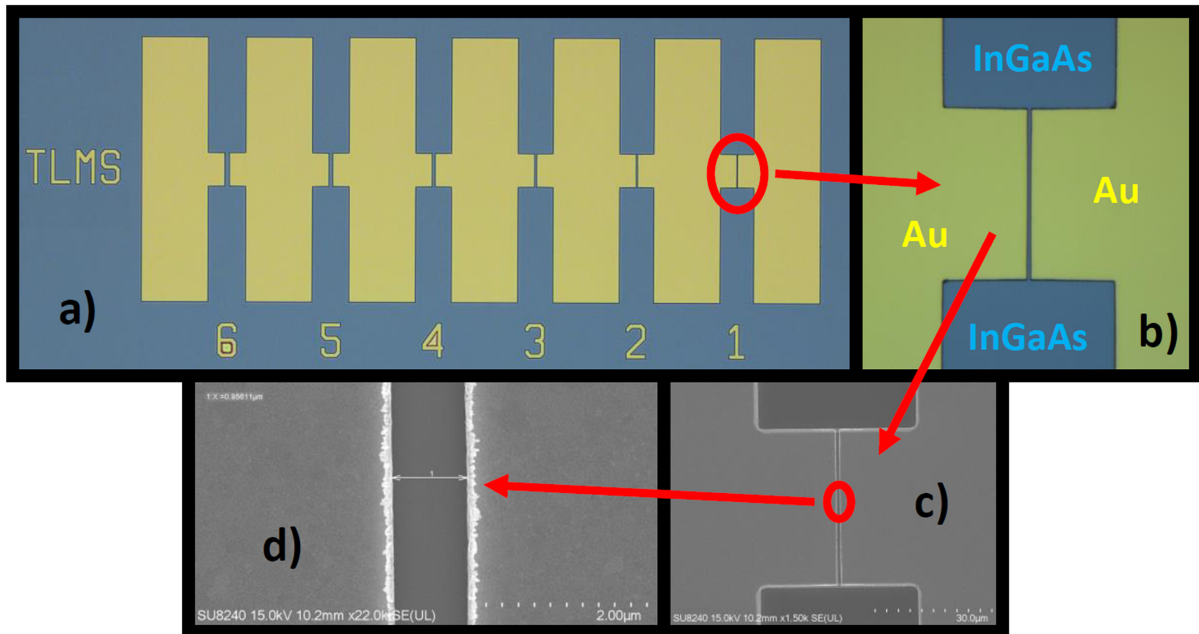

Figure 4. Photomicrographs and SEM images of a TLM structure after lift-off. In **a)**, the whole structure. In **b)**, a zoom in over the 1 μm wide gap area. In **c)**, the 1 μm wide gap seen through SEM. In **d)**, a further zoom in over the gap.

4. CHARACTERISATION OF OHMIC CONTACTS WITH THE PROPOSED TLM STRUCTURE

The fabricated TLM structures were then measured at room temperature to extract ρ_c by using a B1500A Semiconductor Device Parameter Analyzer from Keysight Technologies. Several structures were characterised to get statistical significance. Figure 5 a) shows the employed mask layout, while Figure 5 b), c), and d) report photomicrographs of the 3 μm wide gap measurement area of one of the analysed structures for accurate four-point probe sensing. As it is possible to observe, accurate alignment of the photo-mask for mesa definition was successfully achieved, which eliminates in plane current crowding effects. Within the adopted measurement setup, the bottom probes injected current (I_F), while the top one sensed voltage (V_S), retrieving a resistance value R_k (k = 1, . . ., 6) mainly consisting of twice the contact resistance R_c plus the gap sheet resistance.

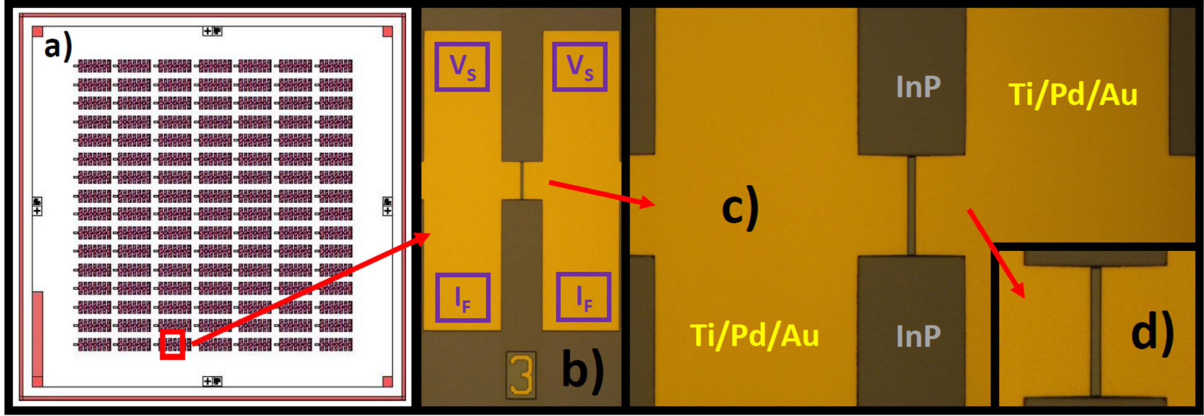

Figure 5. In **a)**, the employed mask design, featuring one hundred and twelve TLM structures. In **b)**, **c)**, and **d)**, photomicrographs of the 3 µm wide gap section of one of the characterised structures, including two zooms in over the gap.

R_c and the transfer length L_t were then extracted through linear fitting over the measured data for all the gaps, as shown in Figure 6, resulting in an estimated $R_c \simeq 0.435$ Ω and $L_t \simeq 0.789$ µm. L_t can be considered as a physical measure of the effective length of the contact or, alternatively, as a characteristic decay length associated with the non-uniform (exponential) spatial distribution of the current flow in/out the contact along the length of the contact itself, so that $R_c = \rho_c/A_{eff} = \rho_c/wL_t$, where A_{eff} and w are the contact effective area and width, respectively. In other words, L_t is, by definition, the inverse of the average time electrons travel below the contact.
Finally, ρ_c was extracted by employing standard TLM theory [12]:

$$\rho_c \approx wR_cL_t \, tanh\left(\frac{d}{L_t}\right) \cong 1.37 \times 10^{-7}\ \Omega\ \mathrm{cm}^2 = 13.7\ \Omega\ \mu\mathrm{m}^2$$

where w = 40 µm and d = 20 µm, being d the length associated with the gaps metal patches. The measured and extracted data are reported in Table 1. The estimated ρ_c was around one order of magnitude higher than state-of-the art values for the same metal stack (≃ 1 Ω µm^2 [19]) due to the unoptimised pre-metal deposition surface de-oxidation cleaning procedure adopted in this work. However, this is about three to six times smaller than state-of-the-art results for high-power RTDs employed in oscillators working in the low-THz range (≃ 45-83 Ω µm^2) [9] [20].

Table 1 Measured and extracted data.

R_1 [Ω]	R_2 [Ω]	R_3 [Ω]	R_4 [Ω]	R_5 [Ω]	R_6 [Ω]	R_c [Ω]	L_t [µm]	ρ_c [Ω µm^2]
≃ 1.44	≃ 1.99	≃ 2.49	≃ 3.06	≃ 3.65	≃ 4.19	≃ 0.435	≃ 0.789	≃ 13.7

5. CONCLUSIONS

We successfully designed and fabricated TLM structures which can be adopted to accurately extract the specific contact resistivity ρ_c associated with metal to heavily-doped n-type InGaAs Ohmics by accounting for state-of-the-art design strategies. We introduced a dual-exposure step based on e-beam lithography which reliably opens gaps down to 1 µm in width, allowing for an accurate extraction procedure. In addition, the structures were used to characterise low-resistance standard contacts used in RTD technology [2] [5] based on a Ti/Pd/Au metal stack, resulting in an extracted $\rho_c \simeq 1.37\times10^{-7}$ Ω cm^2 = 13.7 Ω µm^2 which is, at present, around three to

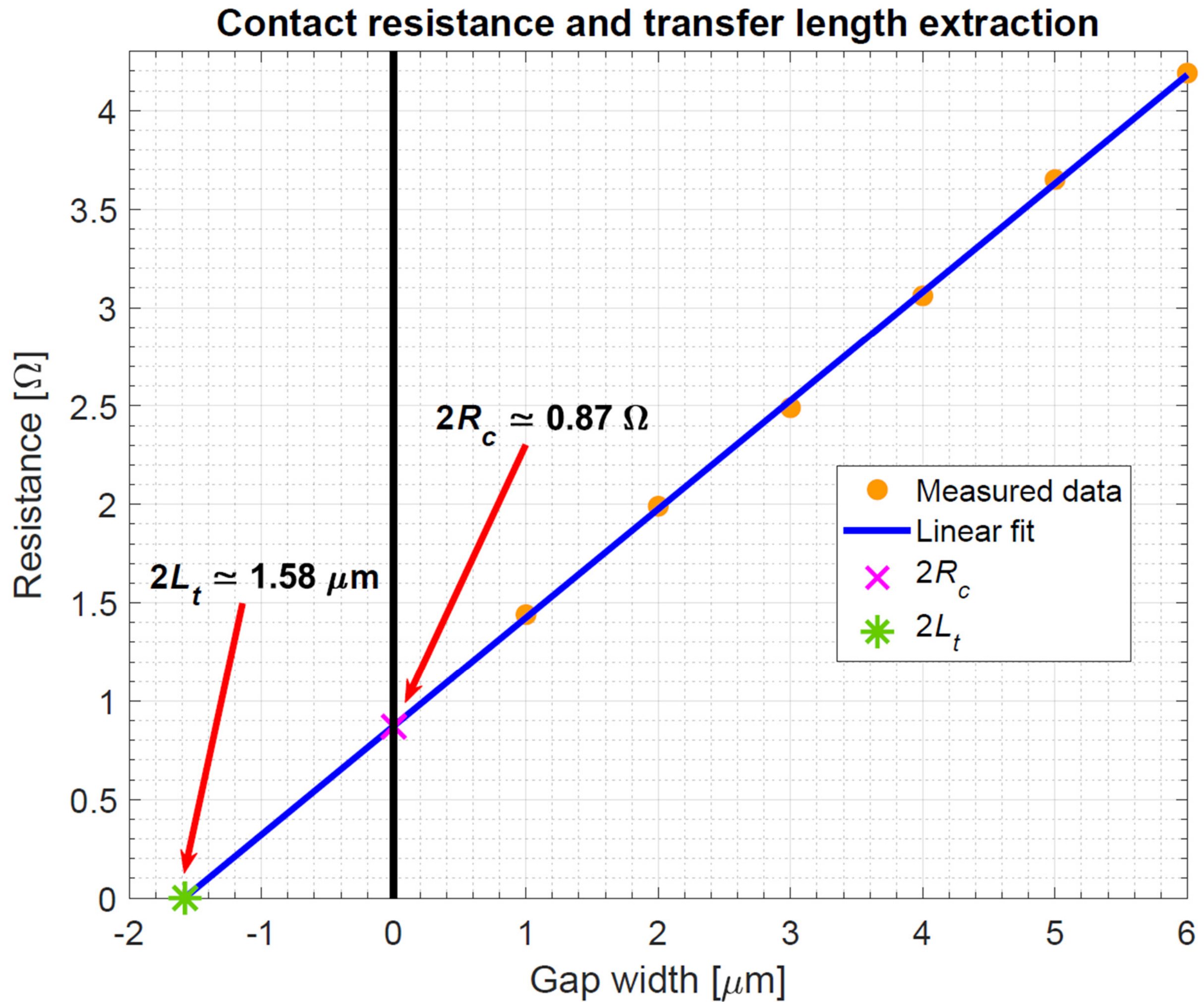

Figure 6. Extraction of the contact resistance R_c and transfer length L_t through linear fitting over the measured data.

six times smaller than reported values for high-power InGaAs/AlAs RTD oscillators operating at low-THz frequencies.

We believe that this work will support in optimising the RTD device Ohmic contacts in order to boost the oscillator RF power. In particular, from an epitaxial design perspective, the InGaAs cap layer has to be engineered to reduce as much as possible the associated Schottky potential barrier occurring at the metal-InGaAs interface, by playing with both the associated indium molar fraction and doping level. Moreover, new metal stacks could be employed, including those based on work function-compatible refractory metals, such as molybdenum [16]-[18]. Indeed, due to its large melting point (~ 2895 K), Ohmic contacts thermal stability rises, increasing device reliability [21]. At the same time, from the fabrication side, optimised ex-situ hybrid-chemical/physical de-oxidation cleaning and thermal annealing procedures [17] need to be developed to efficiently remove the surface native oxide prior to metal deposition, which greatly increases the contacts junction potential barrier. We are confident that, by employing such an optimised processing, ρ_c values in line with state-of-the-art results (~ 10^{-8} Ω cm^2 [16] [17] [19]) will be achieved. Other benefits associated with ρ_c minimisation include spectral line-width narrowing and resonator quality factor enhancement, which diminish the oscillator phase-noise. Together with rising the output power of the transmitter, this will assist in increasing the signal-to-noise ratio, and so increasing the data rate and extending the link distance associated with emerging RTD-based ultra-broadband short-range THz wireless communication systems.

ACKNOWLEDGEMENTS

The authors would like to thank the James Watt Nanofabrication Centre (JWNC) staff, University of Glasgow, for the support during microfabrication. The work of Davide Cimbri was supported by TeraApps (Doctoral Training Network in Terahertz Technologies for Imaging, Radar and Communication Applications), which received funding from the European Union's Horizon 2020 research and innovation programme under Marie Skłodowska-Curie Innovative Training Network (ITN) grant agreement No. 765426.

REFERENCES

[1] M. Feiginov, Journal of Infrared, Millimeter, and Terahertz Waves, vol. **40**, no. 4, pp. 365-394 (2019).

[2] D. Cimbri and E. Wasige, "Terahertz Communications with Resonant Tunnelling Diodes: Status and Perspectives," in Next Generation Wireless Terahertz Communication Networks, 1st Edition, Part I: Terahertz Transceiver and Devices, Chapter 2, CRC Press (2021).

[3] Y. Nishida, N. Nishigami, S. Diebold, J. Kim, M. Fujita, and T. Nagatsuma, Scientific Reports, vol. **9**, no. 1, pp. 18125 (2019).

[4] T. Nagatsuma, IEICE Electronics Express, vol. **8**, no. 14, pp. 1127-1142 (2011).

[5] M. Asada and S. Suzuki, Sensors, vol. **21**, no. 4, pp. 1384 (2021).

[6] C. Kim and A. Brandli, IRE Transactions on Circuit Theory, vol. **8**, no. 4, pp. 416-425 (1961).

[7] E. R. Brown, C. D. Parker, and T. C. L. G. Sollner, Applied Physics Letters, vol. **54**, no. 10, pp. 934-936 (1989).

[8] L. Wang, "Output Power Analysis and Simulations of Resonant Tunneling Diode Based Oscillators," International Computer Science Conference (ICSC): System Simulation and Scientific Computing, pp. 47-55 (2012).

[9] A. Al-Khalidi, K. H. Alharbi, J. Wang, R. Morariu, L. Wang, A. Khalid, J. M. L. Figueiredo, and E. Wasige, IEEE Transactions on Terahertz Science and Technology, vol. **10**, no. 2, pp. 150-157 (2020).

[10] A. Baraskar, A. C. Gossard, and M. J. W. Rodwell, Journal of Applied Physics, vol. **114**, no. 15, pp. 154516 (2013).

[11] J. Maassen, C. Jeong, A. Baraskar, M. Rodwell, and M. Lundstrom, Applied Physics Letters, vol. **102**, no. 11, pp. 111605 (2013).

[12] G. K. Reeves and H. B. Harrison, IEEE Electron Device Letters, vol. **3**, no. 5, pp. 111-113 (1982).

[13] R. Dormaiera and S. E. Mohney, Journal of Vacuum Science & Technology B, vol. **30**, no. 3, pp. 031209 (2012).

[14] G. S. Marlow and M. B. Das, Solid-State Electronics, vol. **25**, no. 2, pp. 91-94 (1982).

[15] J. H. Klootwijk and C. E. Timmering, "Merits and limitations of circular TLM structures for contact resistance determination for novel III-V HBTs," Proceedings of the 2004 International Conference on Microelectronic Test Structures (IEEE Cat. No.04CH37516), pp. 247-252 (2004).

[16] A. Baraskar, M. A. Wistey, V. Jain, E. Lobisser, U. Singisetti, G. Burek, Y. J. Lee, B. Thibeault, A. Gossard, and M. Rodwell, Journal of Vacuum Science & Technology B, vol. **28**, no. 4, pp. C5I7-C5I9 (2010).

[17] S. Masudy-Panah, Y. Wu, D. Lei, A. Kumar, Y. -C. Yeo, and X. Gong, Journal of Applied Physics, vol. **123**, no. 2, pp. 024508 (2018).

[18] A. K. Baraskar, M. A. Wistey, V. Jain, U. Singisetti, G. Burek, B. J. Thibeault, Y. J. Lee, A. C. Gossard, and M. J. W. Rodwell, Journal of Vacuum Science & Technology B, vol. **27**, no. 4, pp. 2036-2039 (2009).

[19] A. M. Crook, E. Lind, Z. Griffith, M. J. W. Rodwell, J. D. Zimmerman, A. C. Gossard, and S. R. Bank, Applied Physics Letters, vol. **91**, no. 19, pp. 192114 (2007).

[20] J. Wang, A. Al-Khalidi, L. Wang, R. Morariu, A. Ofiare, and E. Wasige, IEEE Transactions on Microwave Theory and Techniques, vol. **66**, no. 11, pp. 4698-4705 (2018).
[21] U. Singisetti, M. A. Wistey, J. D. Zimmerman, B. J. Thibeault, M. J. W. Rodwell, A. C. Gossard, and S. R. Bank, Applied Physics Letters, vol. **93**, no. 18, pp. 183502 (2008).